Colloids and Surfaces B: Biointerfaces 241 (2024) 114043

Contents lists available at ScienceDirect

Colloids and Surfaces B: Biointerfaces

journal homepage: www.elsevier.com/locate/colsurfb

Fine-tuning of membrane permeability by reversible photoisomerization of aryl-azo derivatives of thymol embedded in lipid nanoparticles

Samanta Moffa [a], Simone Carradori [a], Francesco Melfi [a], Antonella Fontana [a,b], Michele Ciulla [a,b], Pietro Di Profio [a], Massimiliano Aschi [c], Rafal Damian Wolicki [a], Serena Pilato [a,b,*], Gabriella Siani [a,b,*]

[a] Dipartimento di Farmacia, Università degli Studi Gabriele d'Annunzio Chieti-Pescara, Via dei Vestini 31, Chieti 66100, Italy
[b] UdA-TechLab, Research Center, Università degli Studi Gabriele d'Annunzio Chieti-Pescara, Via dei Vestini 31, Chieti 66100, Italy
[c] Dipartimento di Scienze Fisiche e Chimiche, Università degli Studi dell'Aquila, via Vetoio, Coppito, L'Aquila 67100, Italy

ARTICLE INFO

Keywords:
Photo-responsive liposomes
Azobenzene
trans-cis isomerization
Ion uptake
Drug release
Kinetics

ABSTRACT

Responsiveness of liposomes to external stimuli, such as light, should allow a precise spatial and temporal control of release of therapeutic agents or ion transmembrane transport. Here, some aryl-azo derivatives of thymol are synthesized and embedded into liposomes from 1-palmitoyl-2-oleoyl-*sn*-glycero-3-phosphocholine to obtain light-sensitive membranes whose photo-responsiveness, release behaviour, and permeability towards Cl^- ions are investigated. The hybrid systems are in-depth characterized by dynamic light scattering, atomic force microscopy and Raman spectroscopy. In liposomal bilayer the selected guests undergo reversible photoinduced isomerization upon irradiation with UV and visible light, alternately. Non-irradiated hybrid liposomes retain entrapped 5(6)-carboxyfluorescein (CF), slowing its spontaneous leakage, whereas UV-irradiation promotes CF release, due to guest *trans*-to-*cis* isomerization. Photoisomerization also influences membrane permeability towards Cl^- ions. Data processing, according to first-order kinetics, demonstrates that Cl^- transmembrane transport is enhanced by switching the guest from *trans* to *cis* but restored by back-switching the guest from *cis* to *trans* upon illumination with blue light. Finally, the passage of Cl^- ions across the bilayer can be fine-tuned by irradiation with light of longer λ and different light-exposure times. Fine-tuning the photo-induced structural response of the liposomal membrane upon isomerization is a promising step towards effective photo-dynamic therapy.

1. Introduction

Liposomes are supramolecular architectures widely used as nano-carriers for drug delivery [1] and as versatile biomimetic model systems to study the interactions of biological membranes with molecules and ions.[2] In fact, like the membrane of living cells, the liposomal bilayer constitutes a semipermeable barrier responsible for the selective transport of molecules, being quite impermeable to charged species, including physiologically important anions and cations such as chloride, potassium and sodium, while it is permeable to small, neutral and hydrophobic molecules, that can pass by simple diffusion or through the formation of pores and transient defects.[3,4]

Liposomes are biocompatible, low toxic and able to efficiently encapsulate a large variety of hydrophilic and hydrophobic compounds, such as small-molecule drugs, proteins and nucleic acids.[5–7] Encapsulation increases the solubility of the drug, improves its therapeutic efficacy, prolongs blood circulation time protecting drug from deactivation, and reduces toxic side effects.[8,9] However, the passive release of encapsulated molecules from liposomes is a slow process which is disadvantageous under acute conditions, and it would not allow the drug to reach the desired therapeutic concentration at the target site, limiting its effectiveness. Achieving high levels of spatial and temporal control over transmembrane transport represents a key challenge in membrane technology to obtain high local concentration of drug but low systemic exposure.

Smart liposomal systems have been recently engineered to improve performance in regulating the release and the uptake of molecular or charged species by using internal or external stimuli such as pH, heat, magnetic or electric fields, ultrasound and light.[10–17] Among the triggering modalities for on-demand modulation of bilayer

* Corresponding authors at: Dipartimento di Farmacia, Università degli Studi Gabriele d'Annunzio Chieti-Pescara, Via dei Vestini 31, Chieti 66100, Italy.
E-mail addresses: serena.pilato@unich.it (S. Pilato), gabriella.siani@unich.it (G. Siani).

https://doi.org/10.1016/j.colsurfb.2024.114043
Received 14 March 2024; Received in revised form 7 June 2024; Accepted 15 June 2024
Available online 17 June 2024

permeability, light represents the most attractive option. In fact, light can be easily and remotely applied causing a fast response, can be focused on a specific location, and can offer a precise control of bilayer permeability by simply adjusting parameters such as wavelength, energy and exposure time. Photo-responsive liposomes were obtained from lipids properly modified by covalently linking a photoswitchable group in their lipophilic backbones,[18–20] or embedding a free molecular photoswitch, such as azobenzene,[21–23] stilbene[24] or spyropyran derivatives[25,26] into the liposomal bilayer.

A photoswitch is a molecule that undergoes a reversible change in its physical properties upon absorption of light. The reversibility allows the molecule to potentially act as an on/off switch with an "on" state in one form and an "off" state in the other form.

Liposomes incorporating photoisomerizable lipids have been investigated as potential agents for controlled drug delivery since the early 2000's.[27,28] Most of these systems rely on azobenzene and its derivatives. Upon excitation at around 360 nm, azobenzene undergoes geometric isomerization from the thermally stable, apolar *trans* isomer to the metastable, bent and polar *cis* isomer. The well-separated absorption wavelengths of the two isomers, which ensure that light of a specific wavelength is absorbed by only one of the two isomers, the large geometrical differences between the *cis* and *trans* isomers, the relatively high photostability and easiness of chemical functionalization, the absence of by-products, make azobenzene a powerful photoswitch for numerous applications, from materials science to biology.[29–33] The *trans* isomer is favored in the lipid bilayer where it can pack tightly. Photoisomerization to the *cis* isomer causes the tight packing to be lost, resulting in changes in the structure and properties of the membrane, such as surface area and pressure, layer thickness, shape and fluidity.[34,35]

Recently, photoswitchable giant unilamellar vesicles (GUVs) have been developed from azobenzene-containing phosphatidylcholine (azo-PC) and the mechanisms involved in the on-off triggered structural changes of the lipid bilayer have been in-depth investigated. Vesicle shape transformations such as budding, invagination and tube formation, and even vesicle fission have been observed upon *trans*-to-*cis* photoisomerization, which probably affects the lateral stacking and interaction between the lipids in the membrane.[36,37]

The *trans*-to-*cis* switching of the photoresponsive phospholipids increased the bilayer permeability leading to the leakage of encapsulated molecules through the formation of transient pores.[38] DSPC-cholesterol liposomes incorporating 10 mol% azo-PC and loaded with doxorubicin, exhibited long blood circulation half-lives and up to 80 % light-triggered release upon azo-PC *trans*-to-*cis* switching.[39]

Photoisomerization is a reversible process and illumination with visible light leads to reversion to the *trans* isomer so that the disordered lipid bilayer and content release due to the *trans*-to-*cis* photoisomerization can be reversed by irradiation at λ=455 nm, switching the release off.[40]

Amphiphilic photoisomerizable azobenzene derivatives, non-covalently linked to the phospholipid tails, have also been incorporated into lipid bilayers. For example, 4-butylazobenzene-4-hexyloxy-trimethyl-ammoniumtrifluoro-acetate (BHA) has been inserted into phosphatidylcholine-based lipid nanoparticles, in which curcumin has been encapsulated.[41] The isomerization of BHA upon ultraviolet (UV) irradiation led to the release of approximately 90 % of the loaded curcumin. Light responsive on-off switched release of curcumin was obtained by irradiating alternately with UV and visible light.

The reversible structural changes of photoswitchable molecules inserted into lipid membranes also allowed to study the membrane response to internal conformational changes for controlling ion channel activity.[42] Several azo-derivatives have been designed to act as ion channel agonists and have been shown to be able to control activation and deactivation of these channels by switching from UV-A light to blue light, with high precision.[42–45] Ultimately, the utility of photo-responsive molecular switches in modulating the properties of artificial membranes and their significant potential in photo-pharmacology have become increasingly evident, and, as a result, photo-responsive supramolecular systems are gaining more and more attention.

In this work, we developed light-sensitive supramolecular systems by embedding new synthesized *para*-substituted aryl-azo derivatives of thymol into liposomes from 1-palmitoyl-2-oleoyl-*sn*-glycero-3-phosphocholine (POPC), to obtain suitable tools for manipulating lipid order and dynamics through a reversible light-induced *trans*-to-*cis* isomerization.

In particular, we have investigated the effect of UV light irradiation on the ability of these liposomal systems to release their content, and on the permeability of the bilayer towards chloride ions. Different wavelengths have been chosen to produce the desired photo-stationary state mixture of isomers and to modulate the effect on bilayer permeability. Moreover, the possibility to recover the initial membrane condition by back-switching the guest from *cis* to *trans* has been explored. Molecular dynamics (MD) simulations were also carried out for providing support to our experimental results.

Thymol, a monoterpenoid phenol with multiple biological activities such as expectorant, anti-inflammatory, antiviral, antibacterial, and antiseptic, which is naturally present in essential oils obtained from *thyme* and *oregano*, has been chosen for its ability to integrate into the membrane bilayer with the hydrophilic part of the molecule interacting with the polar heads of the phospholipids, and the hydrophobic benzene ring and aliphatic side chains intercalating within the alkyl chains of the membrane lipids. Thymol incorporation within the membrane causes an increase in membrane permeability, pore formation and membrane damage,[46–49] which are responsible of its antibacterial activity.

The introduction of the azo group makes these derivatives sensitive to light stimuli, leading to a possible additional effect on membrane permeability, due to the structural change upon photoinduced reversible *trans*-to-*cis* isomerization, and offering the opportunity for precise spatial and temporal control. Some aryl-azo derivatives of thymol with significant antibacterial and antifungal activities have been yet synthesized by Swain.[50]

2. Experimental section

2.1. Materials

1-Palmitoyl-2-oleoyl-*sn*-glycero-3-phosphocholine (POPC) was purchased from Avanti Polar Lipids (Alabaster, AL). The fluorescent probes 5(6)-carboxyfluorescein (CF) and lucigenin, azobenzene, $CHCl_3$, CH_3OH, Sephadex G-25 and the salts used for the preparation of buffers were purchased from Sigma Aldrich and used without further purification.

Aryl-azo-thymol derivatives 1–4 were synthesized according to published procedures.[50] All chemicals used were of analytical grade, water was doubly distilled deionized of HPLC grade, and all experiments were carried out with freshly prepared solutions.

2.2. Instruments

Fluorimetric measurements have been carried out on Jasco FP-8200 spectrofluorimeter. UV–vis absorption measurements have been performed on a Jasco V-550UV/Vis spectrophotometer. The size and ζ potential values of liposomal systems were measured by using a 90Plus/BI-MAS ZetaPlus multiangle particle size analyzer (Brookhaven Instruments Corp., Holtsville, NY). AFM analyses have been performed on Multimode 8 AFM (Bruker, Billerica, Massachusetts, US) with Nanoscope V controller, operating in ScanAsyst in air mode.

Raman spectra were obtained by confocal and high-performance Raman microscope (XploRA PLUS, HORIBA, Japan) with deep-cooled CCD detector technology. LabSpec 6.6.1.14 (Horiba, Japan) was employed to control, optimize, and process the acquired data. ^{1}H and

^{13}C NMR spectra were recorded on a Varian VXR-300 spectrometer (Varian Medical Systems, Inc., Paolo Alto, CA, USA).

2.3. Synthesis of aryl-azo-thymol derivatives 1-4

Aryl-azo-thymol derivatives were prepared as reported in Scheme 1. The cLogP values for the azo derivatives 3 and 4 were calculated by means of ChemDraw 22.0.0 (PerkinElmer).

2.3.1. Synthesis of (E)-2-isopropyl-4-((4-methoxyphenyl)diazenyl)-5-methylphenol (1) and (E)-2-isopropyl-5-methyl-4-((4-nitrophenyl) diazenyl)phenol (2)

An acid solution (HCl/H_2O 1/10 mL, v/v) of the proper substituted aniline (6.6 mmol) was added to an aqueous solution of sodium nitrite (9.9 mmol in 5 mL of water) at low temperature (0–5 °C, ice bath). The diazonium salt was allowed to couple by adding a mixture of thymol (6.6 mmol) in an aqueous solution of NaOH (6.6 mmol in 5 mL of water) maintaining the pH value between 8 and 9. When the reaction completed, the mixture was poured into water (30 mL) and extracted with dichloromethane (DCM) for three times (3 ×15 mL). To remove traces of water, anhydrous sodium sulphate (Na_2SO_4) was added to the collected organic layers. The organic phase was evaporated *in vacuo* and the target molecules were recovered through column chromatography, employing silica gel (SiO_2) and proper mixtures of *n*-hexane/ethyl acetate.

2.3.2. Synthesis of (E)-2-isopropyl-4-((4-methoxyphenyl)diazenyl)-5-methylphenyl acetate (3) and (E)-2-isopropyl-5-methyl-4-((4-nitrophenyl) diazenyl)phenyl acetate (4)

Sodium bicarbonate (3.0 equivalents) was added to a solution of azo compounds **1** and **2** (1.0 equivalent) and an excess (4.0 mL) of acetic anhydride. The reaction was allowed to stir at room temperature until the diazo starting material was no detectable on TLC. Once finished, the mixture reaction was evaporated *in vacuo*, to eliminate the excess of Ac_2O and the formed acetic acid, solubilized in DCM and filtrate to remove the salts. The crude product did not need any purification methods.

2.4. Preparation of liposomal systems

Large unilamellar vesicles have been prepared from POPC by the thin film hydration method, following the procedure reported in the literature.[51,52] Briefly, the appropriate amount of a guest stock solution in $CHCl_3$ has been added to a stock solution of POPC in $CHCl_3$ to give a final guest/lipid ratio = 1:10. The mixture was evaporated at 40 °C under reduced pressure and the obtained thin lipid film formed on the wall of the flask was vacuum dried and rehydrated with an appropriate aqueous buffer solution, depending on the type of measurement (release of entrapped dye, passage of chloride ions). After a hydration period of 30 min, the lipid suspension was extruded five times through polycarbonate membranes (pore size 100 nm, Nucleopore Track-Etched Membranes, Whatman, GE Healthcare, USA) mounted on an extruder (Lipex Biomembranes, Vancouver). The extrusion was performed at room temperature.

2.5. Dynamic light scattering (DLS) analysis

For size measurements, the autocorrelation function of the scattered light was analysed assuming a log Gaussian distribution of the liposome size. The mean size and polydispersity index have been obtained. The ζ potential values were calculated from the electrophoretic mobility by means of the Helmholtz-Smoluchowski relationship.

2.6. Atomic force microscopy experiments

Atomic Force Microscopy (AFM) was used in order to investigate the morphology and size distribution of the doped-POPC liposomal systems. The samples were prepared by depositing a drop of diluted suspension of liposomes on freshly cleaved muscovite mica substrates, followed by drying in the oven at 303 K for 2 h and then at room temperature overnight. The obtained samples were scanned by the silicon ScanAsyst-Air probe (triangular geometry, cantilever resonance frequency 70 kHz and nominal spring constant 0.4 N/m) in ScanAsyst in air mode. The AFM images of 512 ×512 pixels were acquired at a scan rate of 1 Hz, collected with different scan sizes and elaborated using Nanoscope Analysis 1.8 software.

2.7. Raman experiments

The Raman spectra of pure POPC liposomes and liposomes doped with the photoswitches, both in their *trans* and *cis* configurations, were obtained after depositing a drop of diluted suspension of liposomes on silicon wafer substrates in a dark environment and measuring with a 532 nm laser and 1800-line/mm grating. All Raman spectra were collected in a spectral range from 2100 to 3050 cm^{-1} and with the same measurement parameters (2 s integration time, 10 accumulations, 25 mW laser power at the samples).

2.8. UV–vis measurements

The reversible photoisomerization process was followed spectrophotometrically in $CHCl_3$, CH_3OH and in POPC liposomes (guest/lipid ratio = 1:10). The final concentration of the photoswitches in the organic solutions was 30 μM. For liposomal suspension, the thin lipid film was rehydrated with a pH = 7.4 buffer prepared from NaCl (174 mM), Na_2HPO_4 (105 mM) and KH_2PO_4 (20 mM). After extrusion, 150 μL of the liposomal suspension were diluted in cuvette to a final volume of 2 mL (final concentration of POPC = 0.5 mM). All steps were carried out in a dark environment.

To induce the *trans*-to-*cis* isomerization process, an in-house built

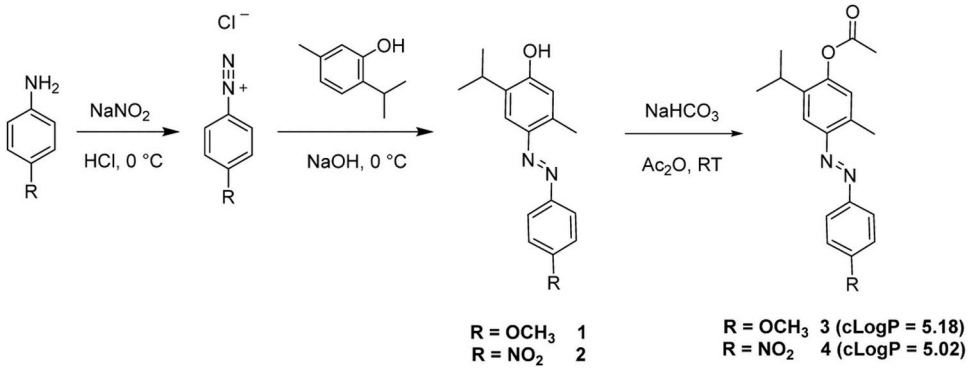

Scheme 1. Synthesis of aryl-azo-thymol derivatives **1–4.**

device with a 2.66 W power light-emitting diode (LED) with emission centered at 365 nm (Mouser Electronics- Munich, Germany) was used and placed in front of a quartz cuvette (1 mm path) containing the solution or liposome suspension. The sample was illuminated uniformly under magnetic stirring. The *cis*-to-*trans* isomerization process was promoted by irradiating the sample with LED lamps centered at 430 nm (0.56 W or 0.14 W) or 530 nm (0.91 W or 0.36 W). After illumination, samples were quickly transferred into the UV–vis spectrophotometer.

2.9. Fluorimetric measurements

Content release experiments have been carried out by using CF as the fluorescent probe. CF (50 mM) was added to the rehydration buffer prepared from NaCl (121.5 mM), Na_2HPO_4 (25.2 mM) and KH_2PO_4 (4.8 mM). The unentrapped dye was removed by passing the liposomal suspension through a Sephadex G-25 column at room temperature, and 4 μL of the liposomal suspension were diluted with an isosmotic buffer (578 mOsm - 174 mM NaCl, 105 mM Na_2HPO_4, 20 mM KH_2PO_4 - pH 7.40) to a final volume of 2 mL (final concentration of POPC = 13.2 μM). The increase in fluorescence emission intensity at $\lambda = 516$ nm, using 490 nm as the excitation wavelength, due to the CF de-quenching which occurs after the leakage of the entrapped CF from the liposomes, was followed over a period of 24 h.

For chloride transport measurements the thin film was rehydrated with a buffer (pH = 6.0) prepared from Na_2HPO_4 (1.4 mM), NaH_2PO_4 (8.6 mM), $NaNO_3$ (100 mM) and lucigenin (1 mM).[53] After extrusion, the unentrapped lucigenin was removed by passing the liposomal suspension through a Sephadex G-25 column, at room temperature. Prior to use, 150 μL of the liposomal suspension were diluted in cuvette to a final volume of 2 mL (final concentration of POPC = 0.5 mM). A concentration gradient across the membrane was created by adding an appropriate amount of a NaCl solution (20 μL, 2.43 M) to the cuvette containing the guest/POPC liposomes, to achieve an external Cl^- concentration of 24 mM.

2.10. Computational details

All the simulations were carried out using the Gromacs package, version 4.5.5.[54] All the species were described adapting the Gromos force-field (gromos53a6) [55] as follows.

For *cis* and *trans* aryl-azo derivatives **3** and **4** (hereafter simply termed as guest) we constructed a force-field through Automated Topology Builder (ATB) [56] re-adapting the atomic charges as obtained from DFT calculations (B3lyp/6–31+G* RESP calculations using Gaussian16).[57] For water we utilized the Simple Point Charge (spc) model.[58] For the POPC membrane (Figure S9) we utilized a bilayer model as obtained from the same repository.

The simulations were then performed in the NVT ensemble, at 298 K, with a time-step of 2.0 fs. The temperature was kept constant using the velocity rescaling thermostat.[59] The LINCS algorithm was employed to constraint all bond lengths.[60] Long-range electrostatic interactions were computed by the Particle Mesh Ewald method with 34 wave vectors in each dimension and a fourth-order cubic interpolation, and a cut-off of 1.8 nm was used.[61] All the simulations were initiated by putting the guest in the center of the membrane and propagated for 200 ns.

2.11. Statistical analysis

Data analysis was carried out with the software package GraphPad Prism 5. To determine the statistically significant differences between the means of independent groups one-way ANOVA with a Tukey post hoc test was used for multiple group comparisons, with p value < 0.05 as a minimal level of significance. All data were obtained from three independent experiments and expressed as mean ± standard deviation (SD). Statistical analysis was performed by comparing the values obtained for *trans* and *cis* isomer for the individual compounds, and, for CF release and Cl^- transport experiments, also by multiple comparisons between all the compounds.

3. Results and discussion

3.1. Photoisomerization properties of aryl-azo derivatives 1–4 in organic solvents

The photoactivity of azobenzene, as reference compound, and the aryl-azo derivatives 1–4 has been investigated in $CHCl_3$, in CH_3OH and in POPC liposomes by means of UV–vis spectroscopy. This technique represents an appropriate tool for studying these systems because the rearrangement of the molecular orbital energy levels, which occurs during isomerization, induces some changes in the absorption spectrum. Indeed, the *trans*-azobenzene absorption spectrum consists of a strong UV band which arises from the symmetry allowed π-π* transition, and a much weaker band in the visible region which corresponds to the symmetry forbidden n-π* transition.[62] In the *cis*-azobenzene absorption spectrum, the intensity of the peak relative to the π-π* transition decreases, while the intensity of the peak in the visible region increases.

The absorption spectrum in CH_3OH of 1, in its *trans* form, shows a strong UV band at $\lambda = 379$ nm and a weak shoulder around 450 nm, while only one absorption band at $\lambda = 396$ nm appears in the absorption spectrum of 2 (Figure S10). Indeed, the two electron repelling substituents, OH and OR, at 4 and 4' positions in 1, as well as the push-pull substitution in 2, cause a red-shift of the π−π* transition and a blue-shift of the n–π* transition, leading the two bands to overlap, even completely in the case of 2.[63,64]

The electronic properties of the substituents also significantly affect the thermal half-life of the *cis* isomer.[65] After irradiation with UV light, only a small change in the absorbance spectrum of 1 occurs, indicating a minimal *trans*-to-*cis* interconversion, and no isomerization is appreciable for 2. This result is in agreement with the evidence already reported in the literature [64,66] that the possibility of charge transfer interactions lowers the energy barrier for *cis*-*trans* thermal interconversion, which completes within milliseconds to seconds, not allowing *trans*-to-*cis* photoisomerization to be observed. The two bands in the UV–vis region, related to the π-π* transition and to the n-π* transition, are well separated in the absorption spectra of the *trans* isomers of 3 and 4 in CH_3OH (Figure S10 d-e). For 3 and 4 the *trans*-to-*cis* conversion was achieved by irradiating the sample at $\lambda = 365$ nm for 5 sec and confirmed by the decrease in intensity of the π−π* band in the UV region, and by the increase in intensity of the n-π* band in the visible region, suggesting that the transformation of the phenolic OH of 1 and 2 into acetate group extends the lifetime of the *cis* isomers of 3 and 4 and allows to reach a *cis*-rich photostationary state. Exposure longer than 5 sec did not lead to further change in the absorption spectrum.

In the dark, the *cis* isomers of 3 and 4 slowly convert back to the *trans* isomers, confirming the reversibility of the process. The *trans* isomer of 3 was restored to about 48 % after approximately 70 h, while the *trans* isomer of 4 was almost completely recovered after approximately 25 h (Figure S11). Absorption spectra of azobenzene and aryl-azo derivatives 1–4 in $CHCl_3$ are reported in Figure S12.

3.2. Photoisomerization properties of aryl-azo derivatives 1–4 in liposomes

The aryl-azo derivatives 1–4 have been embedded into liposomes from 1-palmitoyl-2-oleoyl-*sn*-glycero-3-phosphocholine (POPC), according to the procedure reported in the Experimental Section.

The amount of encapsulated guest was indirectly estimated as the difference between the total weighted guest and the amount of unincorporated guest that remains adhered to the polycarbonate membranes during extrusion, from which the unloaded guest can be easily recovered with CH_3OH and quantified from a calibration curve. The encapsulation

efficiency, EE, expressed by Equation 1:

EE (%) = [(total guest - unincorporated guest) /total guest] x 100%(1)

was determined as 99.12 (± 0.68)%, 96.70 (± 1.55)%, 98.95 (± 0.22)%, 96.81 (± 2.53)% and 33.38 (± 1.54)% for azobenzene, 1, 2, 3 and 4, respectively. All data were obtained from three independent experiments.

Trans-to-*cis* conversion of azobenzene and the aryl-azo-derivatives 3 and 4 was promoted by UV-light illumination also when they were confined into a liposomal bilayer (Figure S13). For 1/POPC and 2/POPC liposomal systems, a *cis*-rich state could not be achieved, due to the short half-life of the guest *cis* isomer, which allows fast and complete restoring of the photoswitch in the dark. We therefore chose to proceed only with the liposomal systems containing azobenzene and the azo-aryl derivatives 3 and 4 for all further investigations.

The reversibility of the *trans*-to-*cis* isomerization process was studied by illuminating the liposomal suspension with blue or green light. Fig. 1a and b show, as an example, the changes in the absorption spectra of 3 embedded into POPC liposomes, on passing from the *cis* isomer to the *trans* isomer upon irradiation at λ = 430 nm (0.14 W) and λ = 530 nm (0.36 W), as a function of time.

Photoswitching from *cis* to *trans* was observed in both cases, but the process is significantly faster ($p < 0.05$) when irradiation is performed at λ = 430 nm, where the absorption of the n−π* transition has a maximum.

The completion of the photoisomerization was measured at the peak of the π→π* band absorbance. The isomerization dynamics were best fitted with a single exponential function, so we assumed the *cis*-to-*trans* conversion to be a first order reaction [67,68] according to the following Equation 2:

$$\ln[(Abs_{eq}\text{-}Abs_0)/(Abs_{eq}\text{-}Abs_t)] = kt \quad (2)$$

where Abs_{eq} and Abs_0 are the absorbances at λ_{max} at equilibrium and t = 0, respectively, while Abs_t is the absorbance value after irradiation, at time t.

The first-order kinetic constants, k_{obs}, for the *cis*-to-*trans* isomerization of azobenzene, 3 and 4 in liposomes have been calculated and collected in Table 1. The photoisomerization at λ = 430 nm and LED's power = 0.56 W was too fast to be followed, for all liposomal systems.

For all the systems, *cis*-to-*trans* isomerization at λ = 530 nm is

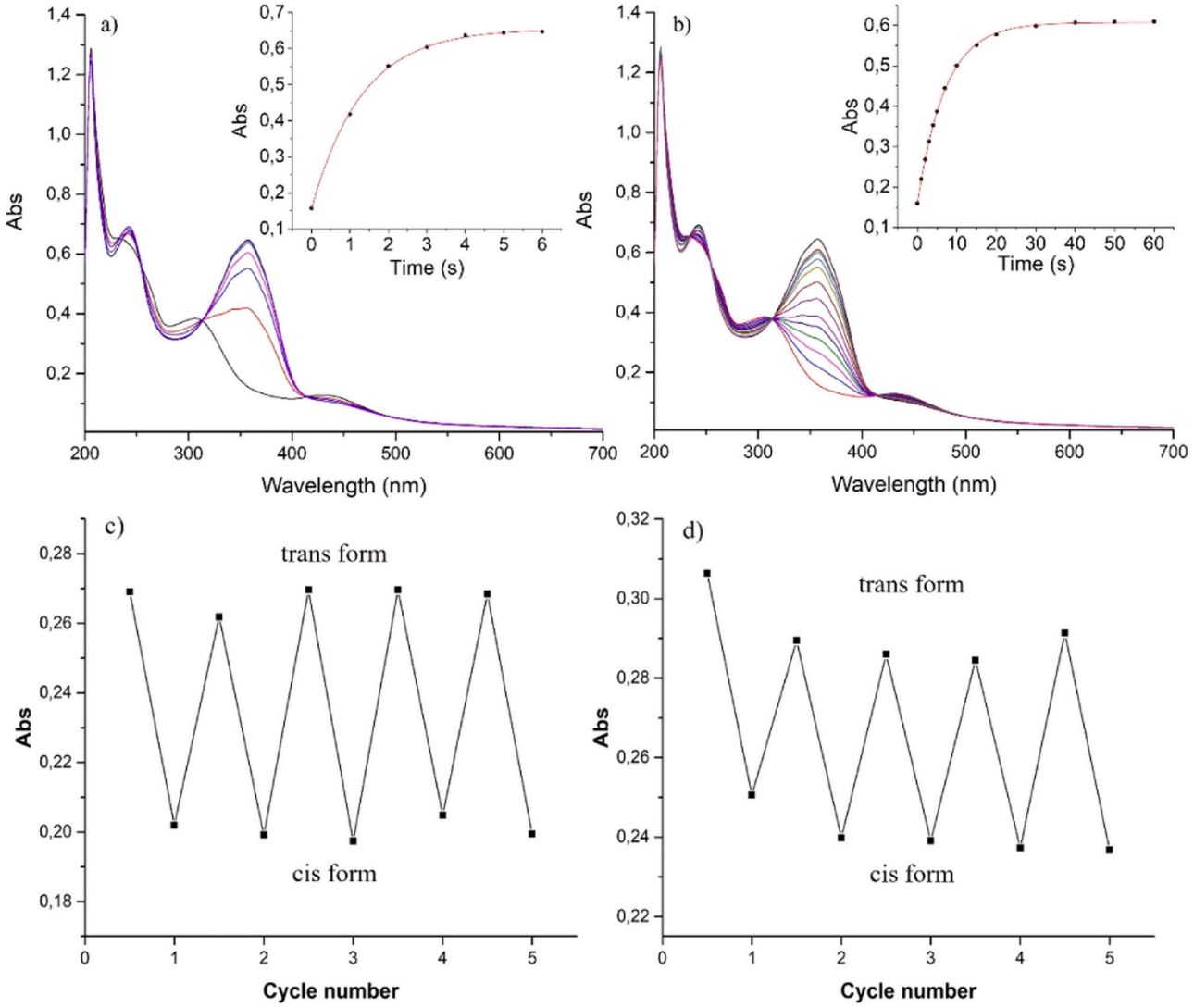

Fig. 1. a) Absorption spectra of the aryl-azo derivative 3 embedded in POPC liposomes upon irradiation at λ = 430 nm or b) λ = 530 nm; each measurement was carried out after 1 second irradiation The insets represent the kinetic profiles for the *cis*-to-*trans* isomerization obtained by plotting the absorbances at λ = 357 nm as a function of irradiation time. c) Absorbance values at λ = 357 nm of the aryl-azo derivative 4 embedded in POPC liposomes under the alternate irradiation at λ = 365 nm and λ = 430 nm/0.56 W or d) under the alternate irradiation at λ = 365 nm and λ = 530 nm/0.91 W; each measurement was carried out after 5 minutes irradiation.

Table 1
Pseudo-first order rate constants for the *cis*-to-*trans* isomerization of azobenzene (Azo) and the aryl-azo derivatives 3 and 4 embedded into POPC liposomes, at 430 and 530 nm, at different LED's power.

	k_{obs} (s^{-1})		
wavelength (LED's power)	Azo/POPC liposomes	3/POPC liposomes	4/POPC liposomes
430 nm (0.14 W)	1.11 ± 0.07	0.639 ± 0.015	0.820 ± 0.015
430 nm (0.56 W)	-	-	-
530 nm (0.36 W)	0.068 ± 0.004	0.142 ± 0.001	0.257 ± 0.013
530 nm (0.91 W)	0.151 ± 0.009	0.352 ± 0.008	0.324 ± 0.013

significantly less efficient ($p < 0.05$, Figure S14) than the fast photoswitching which occurs upon irradiation at λ = 430 nm, i.e. the λ of maximum absorption of the n-π* transition. The rate of the back isomerization is also affected by illumination intensity so that it can be controlled by varying the output power of the LED. These results suggest that azobenzene, 3 and 4 can be used as photo-responsive agents when intercalated into membranes and that the back-switching process can be tuned simply by choosing different irradiation wavelengths and LED's powers.

Photoswitching has been repeated by using alternating UV and blue or green light. The absorbances returned to almost the original values when the liposomal systems were irradiated with light at λ = 430 nm, suggesting that the membrane was not irreversibly damaged over multiple switching cycles. However, the *trans* isomer was not fully restored upon irradiation at 530 nm (Figs. 1c, 1d, and Figure S15).

3.3. Characterization of azobenzene/POPC, 3/POPC and 4/POPC liposomal systems

3.3.1. Particle shape, size and zeta potential

The insertion of guests into the liposomal bilayer may alter lipid packing and liposome morphology, leading to changes in the physicochemical properties of the membrane.[51,53] The size and the ζ potential of the liposomal systems have been determined by DLS at a guest/lipid ratio = 1:10. Values obtained for pure POPC liposomes are also reported for sake of comparison. Sizes and zeta potentials have been measured before and after UV irradiation to assess the morphological sensitivity of the hybrid systems to the light-induced isomerization of the photoswitches. The measured mean diameters and ζ potential values are listed in Table S1.

DLS confirmed the presence of particles whose diameters are consistent with the existence of liposomal assemblies, suggesting that the insertion of the guests does not result in liposome disruption, i.e. liposomes retain their structural integrity. However, a significant increase ($p < 0.05$) in the mean diameter of azobenzene/POPC liposomal system (155 ± 1 nm) was observed with respect to pure POPC liposomes (118 ± 1 nm).

Indeed, it is known that azobenzene can intercalate into the liposomal bilayer through hydrophobic interaction, increasing its density and lateral rigidity, and decreasing its lateral compressibility and bendability.[69] These effects can account for the observed increase in the liposome mean diameter. A less marked size increase occurred when the azo-aryl derivative 3 was embedded within the bilayer (131 ± 1 nm), while liposome diameter was not significantly ($p > 0.05$) influenced by the presence of the azo-aryl derivative 4, probably due to its poor loading efficiency.

Liposome size was slightly reduced after isomerization (Table S1). This result appears to be in contrast with the increase in the cross-sectional area per lipid of azo-PC, observed by Langmuir-Blodgett measurements, [38] and with the increased size and shape deformation of giant unilamellar vesicles (GUVs) from azo-PC, observed by microscopy.[70,71] However, while in these model systems azobenzene is covalently linked to the acyl chain of the phospholipid, so that *trans*-to-*cis* conversion alters the geometry of the lipid molecule, affecting its packing parameters, in the hybrid liposomal system covered by this work, azobenzene is inserted into the bilayer as free molecular switch. In agreement with our results, a size reduction of liposomes doped with free caffeic acid phenethyl ester was demonstrated by Sharma who suggested that the UV-induced *trans*-to-*cis* isomerization within the membrane brings the lipid head groups of the outer and the inner leaflets closer to each other.[72] The thinner membrane of a smaller vesicle suggests that the bilayer may have an interdigitated structure or an orientational disorder conformation.[73] The *trans*-to-*cis* conversion could disturb the compact and well-ordered structure of the bilayer composed of POPC and guest in its *trans* form, causing defects in the membrane that can facilitate water expulsion from liposomes.

ζ potential value is useful to quantify the degree of repulsion between charged particles in the dispersion. The high absolute values of ζ-potential obtained for the studied systems (Table S1) suggest a high kinetic stability as they play a key role in avoiding particle aggregation.[74]

3.3.2. AFM analysis

AFM microscopy represents a suitable method for size detection of polydisperse samples like liposomal suspensions. In Fig. 2 is reported, as an example, the AFM 2D height channel of diluted POPC liposomes enriched by the aryl-azo derivative 4. Most of the vesicles showed a globular and flattened shape, probably due to the alteration induced by the drying step. The horizontal distances calculated for different vesicles (Fig. 2 and S16), of all the tested liposomal systems, are in good agreement with DLS measurements (Table S1), considering that AFM provide reliable and precise information on particle shape, rather than particles size, due to the sample preparation issue, tip convolution and the smaller number of particles analysed by AFM.

A comparison between liposomes containing the guest in its *trans* and *cis* form was not possible because, as shown by DLS measurements (Table S1), the difference in the mean diameter between the two liposomal systems is small (a few nanometers) and, therefore, it is not appreciable by AFM, due to the flattening and/or shrinking that can occur during the drop casting and drying process for sample preparation.

3.3.3. Raman analysis

Raman spectroscopy is a particularly suitable technique for characterizing lipid membrane and investigating the alteration of membrane structure and fluidity induced by the incorporation of guests within the bilayer.[75–77] We focused on the hydrocarbon chain C-H stretching mode region between 2800 cm^{-1} and 3050 cm^{-1} of the Raman spectrum (Figures S17 and S18). This spectral region allows to monitor the behaviour of the phospholipid acyl chains within the bilayer as three well defined peaks can be identified: two peaks at approximatively 2850 cm^{-1} and 2880 cm^{-1}, assigned to the symmetric C-H methylene stretching ($\nu_s(CH_2)$) and to the asymmetric C-H methylene stretching ($\nu_a(CH_2)$), respectively, and a peak at approximatively 2930 cm^{-1}, assigned to the symmetric C-H terminal methyl stretching ($\nu_s(CH_3)$). The height intensity ratios $I_{\nu s(CH3)}/_{\nu a(CH2)}$ and $I_{\nu s(CH3)}/_{\nu s(CH2)}$ are sensitive to the lateral packing density and intermolecular lipid chain order in the lipid acyl chains. The incorporation of a guest into the bilayer can influence acyl chain conformation and packing and, consequently, the values of the ratios. In particular, an increase in $I_{\nu s(CH3)}/_{\nu a(CH2)}$ value indicates a decrease in intramolecular (gauche/trans) and intermolecular (chain packing) interaction; an increase in $I_{\nu s(CH3)}/_{\nu s(CH2)}$ value indicates an increase in rotational disorder and freedom of motion. The differences in the Raman spectrum of each liposomal system with respect to the spectrum of pure POPC liposomes have been analysed and the height intensity ratios have been calculated and reported in Table S2. Results show that the peak intensity ratios $I_{\nu s(CH3)}/_{\nu a(CH2)}$ and $I_{\nu s(CH3)}/_{\nu s(CH2)}$, calculated for azobenzene/POPC liposomes, decrease of ca. 13 % and 11 %, respectively, in relation to those obtained from the spectrum of pure POPC liposomes, indicating that azobenzene induces an increase in both intramolecular and intermolecular interactions, and

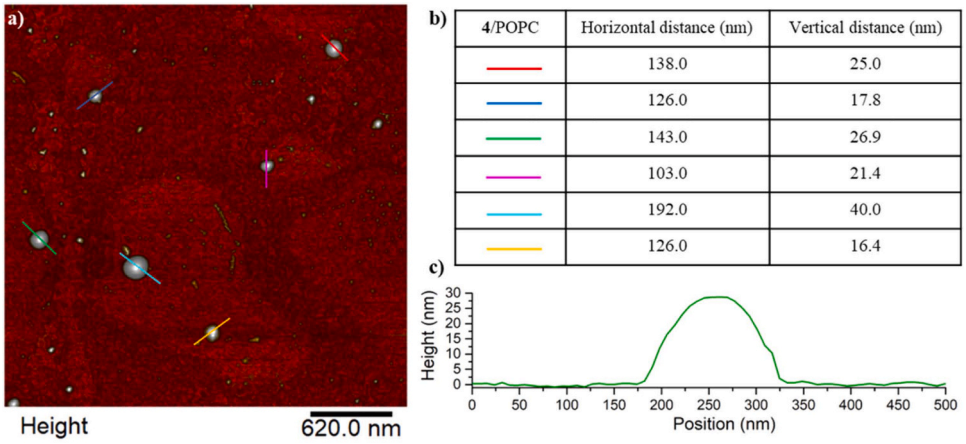

4/POPC	Horizontal distance (nm)	Vertical distance (nm)
	138.0	25.0
	126.0	17.8
	143.0	26.9
	103.0	21.4
	192.0	40.0
	126.0	16.4

Fig. 2. AFM representation of topography of 4/POPC liposomes. In the Table (b) the horizontal and vertical distances related to each marked liposome were listed. The height cross sectional profile of a representative liposome is also reported (c). AFM micrographs of pure POPC, azobenzene/POPC and 3/POPC liposomal systems are shown in Fig. S16.

a decrease in the rotational disorder. The azo-aryl derivatives 3 and 4 show a much milder but opposite effect on liposomal bilayer, compared to azobenzene.

Comparing the height intensity ratio values obtained from the spectra of the *trans* and *cis* forms, a significant increase in $I_{\nu S(CH3)}/_{\nu S(CH2)}$ is evident for 3/POPC (+15.5 %, $p < 0.05$, Figure S19) and 4/POPC (+18.4 %, $p < 0.05$, Figure S19) and, to a lesser extent, for azobenzene/POPC (+3.7 %) liposomal systems, indicating that the *trans*-to-*cis* isomerization induces increase in the rotational and vibrational freedom of the terminal CH_3 groups.

3.4. Computational analysis

MD simulations were performed to highlight possible differences in the behaviour of the *trans* and *cis* isomers of **3** and **4** incorporated into the liposomal bilayer.

The guest was put at the center of the membrane and allowed to freely move. In Fig. 3 the obtained distribution of the photoswitch along the axis normal to the membrane, normally termed as *z*-axis, has been reported. It is important to note that in Fig. 3 a symmetry operation has been adopted, i.e. the guest position below and above the center of the membrane has been considered as invariant. In other words when the guest is found at $+\Delta z_1$ or $-\Delta z_1$ these two formally different states are both considered as representative of $+\Delta z_1$ condition.

Results clearly show significant differences between the *cis* and *trans* forms of the guests. In particular, the *cis* isomers, which systematically (and irrespectively to the nature of the substituent, i.e., nitro- or methoxy-group) show higher dipole moment with respect to the *trans* isomers, are found to stably reside in the more polar membrane/solvent interface.

3.5. Release of 5(6)-carboxyfluorescein

CF is a fluorescent probe often used as a model of hydrophilic drug to test the ability of supramolecular structures to load molecules into their aqueous cores and act as drug carriers. Since for 1 and 2 the *cis* stability is too low to achieve an efficient isomerization, while the ideal would be if the on/off state of the photoswitch could be maintained long enough to allow spatio-temporal control of drug release from liposomes, the experiments on the effects of photoisomerization on liposomal membrane permeability towards CF were conducted only for the photo-responsive liposomal systems containing azobenzene and the azo-derivatives 3 and 4.

However, since the rate of CF leakage from the irradiated system could be potentially affected by the spontaneous *cis*-to-*trans* reconversion which occurs over time, we first investigated the dark *cis*-to-*trans*

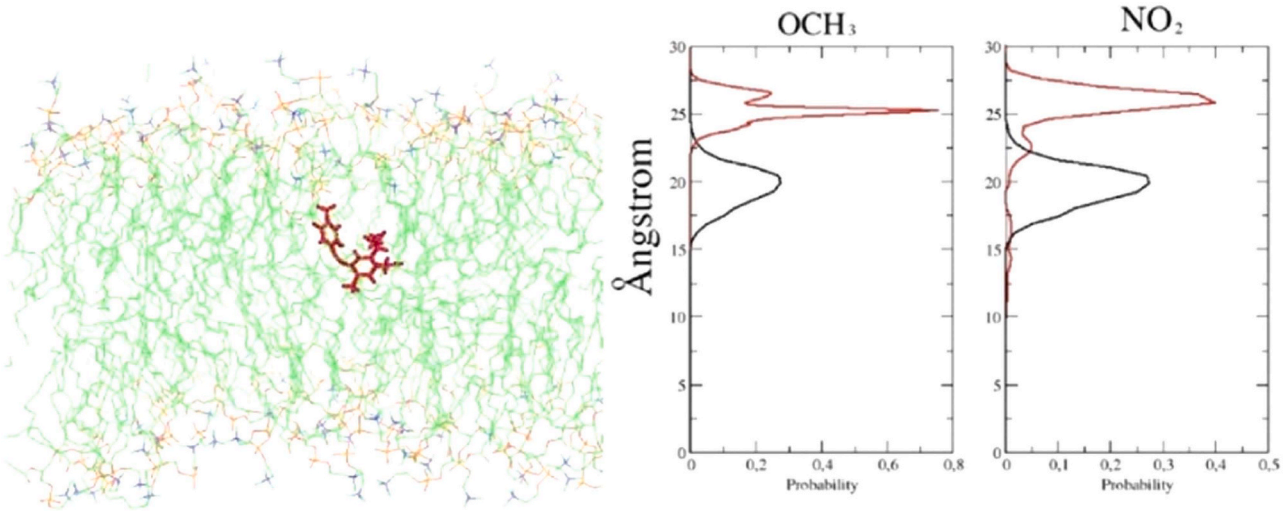

Fig. 3. Normalized distribution function of the photoswitch center of the mass along the membrane normal axis; *cis* and *trans* isomers are reported in red and black, respectively. Note that we adopted a symmetry operation in order to make the result clearer.

back isomerization in liposomes, to evaluate whether this process could interfere with CF leakage measurements.

The dark *cis*-to-*trans* isomerization in liposomes is very slow for azobenzene and for the azo-aryl derivative 3, as neither fully returned to the *trans* form after 24 hours (Figure S20). The *cis* isomer of the azo-aryl derivative 4 converted back to the *trans* isomer over 10 hours, following a first-order kinetics, for which a $k_{obs} = 5.39\ (\pm\ 0.05)\ x10^{-5}\ s^{-1}$ can be calculated.

The CF release from the internal aqueous core of the liposome, which is supposed to occur through the formation of pores and defects in the phospholipidic bilayer,[4,52] was determined fluorimetrically by monitoring the increase in fluorescence of the dye before and after UV irradiation, as described in the Experimental Section. Indeed, the fluorescence of CF is quenched if the dye is locally concentrated into liposomes, while de-quenching occurs upon dilution when CF is released from liposomes into the bulk solution. Control experiments with non-photoswitchable pure POPC liposomes were carried out to ensure that UV irradiation had no influence on phospholipids. Examples of kinetic profiles of the CF release from the hybrid liposomal systems, before and after UV irradiation are reported in Figure S21.

To describe the release behaviour, two different kinetic models were used to fit the release profiles: a first-order kinetic model, according to the general rate expression (Eq. 3):

$$[CF]_{eq} - [CF]_t = Ae^{-t/k_{obs}} \quad (3)$$

and a double-phase kinetic model, which takes into account two release steps and for which the kinetic Eq. 4 was the following:

$$[CF]_{eq} - [CF]_t = Ae^{-t/k_1} + Be^{-t/k_2} \quad (4)$$

where $[CF]_{eq}$ and $[CF]_t$ are the total concentrations of CF released at equilibrium and at time t, respectively, and k_1 and k_2 are the rate constants for the first and the second release step, respectively. The correlation coefficients (R^2) have been calculated to evaluate the goodness of the fits.

The ambiexponent model proved to be the most accurate one ($R^2 \geq 0.999$), suggesting that a two-phase release mechanism occurs. The values of the rate constants, k_1 and k_2, for the biphasic CF release from liposomal systems, before and after UV irradiation, are reported in Table 2. The dark *cis*-to-*trans* back isomerization has been neglected as it is slow enough not to interfere with the measurements of the rate of CF release.

The biphasic leakage of CF from liposomes is characterized by a rapid release in an early stage (burst phase) and a slow release in a later stage (sustained phase). Interestingly, the rate of the sustained release is almost the same for all the studied liposomal systems and irradiation does not lead to any significant effect on the kinetic constants ($p > 0.05$). This result suggests that the sustained phase is independent of liposome composition and the applied stimulus. In contrast, it is evident from Table 2 that the insertion of guests **3** and **4** and *trans*-to-*cis* photoisomerization significantly affects the kinetics of the burst CF release ($p < 0.05$, Figure S22).

Table 2
Rate constant values, k_1 and k_2 for the biphasic release of CF from the investigated liposomal systems before (guest in *trans* form) and after (guest in *cis* form) irradiation with light at $\lambda = 365$ nm.

	$10^{-4}\ k_1\ (s^{-1})$		$10^{-4}\ k_2\ (s^{-1})$	
Liposomal system	*before UV irradiation*	*after UV irradiation*	*before UV irradiation*	*after UV irradiation*
pure POPC	1.87 ± 0.03	1.92 ± 0.02	0.257 ± 0.005	0.202 ± 0.004
azobenzene/POPC	1.77 ± 0.05	2.14 ± 0.13	0.259 ± 0.018	0.196 ± 0.009
3/POPC	0.678 ± 0.04	1.65 ± 0.03	0.250 ± 0.044	0.276 ± 0.041
4/POPC	0.666 ± 0.04	1.51 ± 0.04	0.213 ± 0.055	0.262 ± 0.016

Membranes doped with guests in their *trans* form are less permeable to CF than pure POPC membrane. The permeability of membrane depends on membrane order and on the formation of pores and nanochannels. The absence of any correlation between the order of the membrane resulting from Raman analysis and the rate of CF release suggests that the observed difference in k_{obs} values is mainly due to difference in the distribution of pores or channels in the bilayer rather than to difference in membrane order. A possible explanation could be that guests **3** and **4** in their *trans* form can give rise to interactions between the quaternary ammonium ions on POPC molecules of the inner surface of liposomes and the lone pairs present on the nitrogen atoms of the azo moiety.[23] The results obtained, rationalized also in the light of previous studies present in the literature (see references throughout this section), have led us to suggest that these interaction can hinder the formation of transient pores or defects in the bilayer, thus lowering the efflux of CF. The possibility of π-π stacking interactions between the aromatic rings of guests in their *trans* form and CF can also contribute to slowing probe release.

k_1 values reported in Table 2 show that the *trans*-to-*cis* conversion results in an increase in rate of CF release for all the guest-doped liposomal systems. Presumably, the configurational change from the *trans* form to the bulky and polar *cis* form, which tends to move towards the more polar membrane/solvent interface (Fig. 3), could interfere with the bilayer packing because of lateral area fluctuations, favouring CF release through the formation of transient pores or channels due to the empty spaces generated by the altered guest's shape and its translation within the bilayer.[23,38] Indeed, Raman experiments showed that the *trans*-to-*cis* conversion led to an increase of the $I_{\nu s(CH3)}/_{\nu s(CH2)}$ values, for liposomes embedded with **3** and **4** (15 % and 18 %, respectively), pointing to an increased disorder. Moreover, the above mentioned interactions, especially π-π stacking, are hindered when the guest assumes the *cis* configuration, with consequent acceleration of the release of liposome content. Boruah et al. came to a similar conclusion to explain the effect of light on the release of doxorubicin from phosphatidylcholine-azobenzene nanocomposite vesicles.[23] The rate constant for CF release from non-photoswitchable pure POPC liposomes did not change upon UV irradiation, ensuring that the light stimulus had no effect on the organization of the phospholipid molecules within the bilayer.

3.6. Membrane permeability towards chloride ions

The transmembrane transport of Cl^- ions into liposomes, following the creation of a concentration gradient across the bilayer by addition of NaCl to the liposomal solution, has been evaluated, before and after UV irradiation, by monitoring the fluorescent signal of lucigenin which is quenched upon Cl^- binding. Repeated irradiation experiments were conducted under the alternate irradiation of UV and visible light to test the ability of the guests to act as smart valves in an on/off switch mode. Since illumination wavelength and the irradiation time may influence the rate and degree of isomerization and, consequently, the degree of membrane reorganization, the back *cis*-to-*trans* switching was achieved by varying irradiation wavelength and exposure time. The kinetic profiles of lucigenin quenching for **4**/POPC liposomes are illustrated in Fig. 4, as an example.

Time profiles are consistent with a first-order kinetic mechanism and apparent first-order rate constants, k_{obs}, have been determined. The obtained values are reported in Table 3. Control experiment with pure POPC liposomes confirmed that light irradiation has no significant effect ($p > 0.05$) on membrane permeability in absence of the guests.

The comparison of data in Table 3 with those reported in Table 2 shows that there is no correlation between Cl^- transport and CF release, with the former being approximately two- to three-orders-of-magnitude faster than the latter. However, this result is not really surprising since

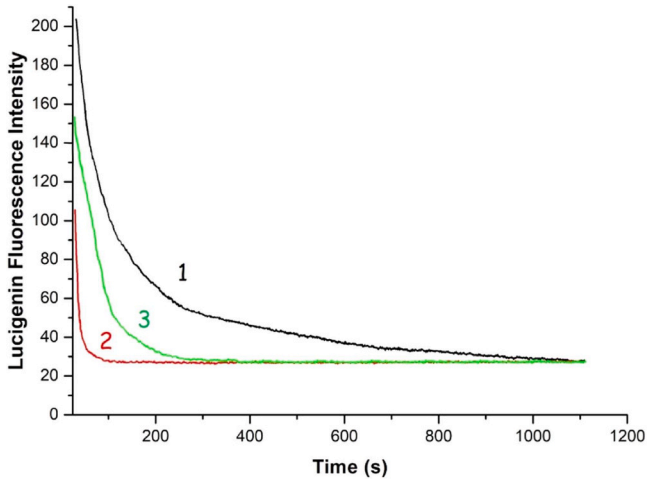

Fig. 4. Kinetic profiles of lucigenin quenching at 298 K, after addition of NaCl to **4**/POPC liposomal suspension. 1: *trans* photostationary state; 2: after *trans*-to-*cis* isomerization upon UV irradiation; 3: after back *cis*-to-*trans* isomerization upon irradiation with visible light at λ = 530 nm, for 2 seconds.

Table 3
First-order rate constants, k_{obs}, for the quenching of lucigenin induced by Cl^- in the investigated liposomal systems and in pure POPC liposomes. Photoswitching has been repeated by using alternating UV and blue or green irradiation.

		$10^{-2}\ k_{obs}\ (s^{-1})$			
Irradiation (nm)	**Photoswitching**	**4**/POPC	**3**/POPC	Azobenzene/POPC	pure POPC
No irradiation	-	0.99 ± 0.08	15.3 ± 0.3	6.78 ± 0.12	0.19 ± 0.08
365	*trans - cis*	13.0 ± 0.7	20.8 ± 0.2	6.97 ± 0.08	0.20 ± 0.07
365–430	*trans - cis - trans*	1.11 ± 0.21	15.7 ± 0.1	-	0.20 ± 0.05
365 – 430 – 365	*trans - cis - trans - cis*	14.6 ± 0.8	21.4 ± 0.3	-	-
365–530 (2 s)	*trans - cis- trans*	2.01 ± 0.11	16.7 ± 1.0	-	-
365–530 (10 s)	*trans - cis- trans*	1.63 ± 0.11	16.5 ± 0.3	-	-

the two processes presumably occur through different mechanisms, as evidenced by the different kinetics (ambiexponential for CF release and first-order for Cl^- transport).

Compared with $k_{obs} = 0.19 \times 10^{-2}\ s^{-1}$, previously reported for pure POPC liposomes,[54] k_{obs} values reported in Table 3 show that all guests in their *trans* form favour Cl^- transport across the liposomal bilayer. A non-specific mechanism related to the perturbation of the bilayer induced by the guest insertion could come into play. Furthermore, the unconventional and non-covalent interaction between anions and π systems could lower the energy barrier for anion-selective transmembrane transport.[78–80]

It may seem surprising that the interaction between the Cl^- ions and the aromatic ring of *trans*-**4**, which is the most electron deficient among all the studied guests, is the least effective. Actually, the lower k_{obs} value obtained for *trans*-**4** compared to the other guests may be due to its lower percentage of incorporation as well as to the fact that, as anion recognition by anion–π interactions has to be combined with anion translocation, a tight binding could decelerate rather than accelerate the ion transfer.[81]

Starting from the *trans* photostationary state, the membrane permeability towards Cl^- ions was increased when photoisomerization to the *cis* photostationary state occurred, especially for **4** and, to a lesser extent, for **3** ($p < 0.05$, Figure S23), despite the lower EE for guest **4** than for guest **3**. Once again, the increase in membrane permeability that follows *trans*-to-*cis* isomerization can be explained in terms of the disturbance that the sudden change in molecular configuration causes to the geometrical packing of the bilayer, resulting in membrane fluctuations which may produce voids and opening between phospholipids. Furthermore, the results from computational analysis also qualitatively support the hypothesis that the possible differences observed in the membrane permeability might be related to the actual position of the guests in their *trans* or *cis* form along the membrane (see Fig. 3).

POPC liposomes doped with the aryl-azo derivatives **3** and **4** were found to have excellent intermittent response. A reproducible cyclic change in membrane permeability towards Cl^- ions was observed upon repeated irradiation with UV light of 365 nm for the *trans*-to-*cis* isomerization and visible light of 430 nm for the *cis*-to-*trans* isomerization. The photoswitching has been repeated twice without significant sign of desensitization and the calculated k_{obs} value always reached its initial value. This result suggests that the photoswitch can reorient itself within the membrane, leading to a lipid reorganization, closing of pores and a complete reversion of membrane response.

In Section 3.2, we showed that *cis*-to-*trans* isomerization is significantly less efficient upon irradiation at λ = 530 than at λ = 430 nm. Therefore, liposomes containing the guest in its *cis* form were also irradiated with light at λ = 530 nm for 2 or 5 seconds, in order to evaluate whether these parameters could be factors regulating the transmembrane transport of Cl^- ions. Rate constants reported in Table 3 show that irradiation with lower energy/higher wavelength light does not allow the membrane to be completely restored as occurs upon irradiation with higher energy/shorter wavelength light, and that membrane permeability towards Cl^- ions can also be modulated by varying the irradiation time.

4. Conclusion

Some optical photoswitches based on azobenzene and thymol structures have been synthesized to be potentially used as light-controllable "smart valves" in liposome bilayers. The guests have been successfully embedded into POPC liposomes and the physicochemical properties of the hybrid systems have been studied. Irradiation with UV light stimulated perturbation within the hybrid membranes due to the reversible *trans*-to-*cis* isomerization of the N═N double bond. We found that the nature of the substituents attached to the azobenzene moiety have a great influence on both optical properties and membrane-modulation ability of the photoswitch. Since the presence of free -OH on the thymol moiety did not allow the *trans*-to-*cis* isomerization to be appreciated, neither in organic solvents nor in liposomes, the alcohol group was, necessarily, acetylated.

CF was encapsulated in liposomes as a model drug, and the release kinetics was studied. Compared to pure POPC liposomes, the guests, in their *trans* form, provided a somewhat inhibitory effect towards CF release. However, the release increases when guests are converted by irradiation into their *cis* form. This behaviour can be aimed at avoiding the slow and spontaneous leakage of the liposomal content before the target site is reached, and then promoting its release with a high spatio-temporal control. Interestingly, photo-stimulated release from liposomes can be achieved in a very low light-exposure time (few seconds), which is particularly useful for limiting any exposure damage.

Photoswitching also controlled the membrane permeability towards ions. The studied photoswitches can activate the transmembrane transfer of Cl^- ions, presumably through the opening of pores or defects in the bilayer following *trans*-to-*cis* isomerization upon optical stimulation with UV light. The reversibility of the process allows membrane properties to be fully restored and the rate of Cl^- influx to return to the initial values, by irradiation with visible light. The transmembrane transport of Cl^- ions could be fine-tuned in response to irradiation with different wavelengths and different exposure times, by controlling the fraction of molecules that are switched to the *trans* or *cis* state. This work will potentially allow to design and develop simple and effective

photoswitches, not necessarily covalently linked to membrane lipids, to tune membrane permeation, thereby controlling the dynamics of ion transport across membranes and drug release for smart delivery and paves the way for further implementation in this field of research.

We are aware of the fact that UV and blue light do not penetrate deeply into tissues, however the studied liposomal systems could be useful in phototherapy for skin, eyes and mucous membranes. Furthermore, the applicability of these systems could be easily expanded by introducing appropriate substituents on the azobenzene unit, that make the photoswitch responsive to NIR light.

CRediT authorship contribution statement

Samanta Moffa: Methodology, Investigation. **Simone Carradori:** Investigation. **Francesco Melfi:** Investigation. **Antonella Fontana:** Funding acquisition, Data curation. **Michele Ciulla:** Visualization. **Pietro Di Profio:** Validation. **Massimiliano Aschi:** Writing – original draft, Investigation, Formal analysis. **Rafal Wolicki:** Investigation. **Serena Pilato:** Writing – original draft, Visualization, Methodology, Investigation. **Gabriella Siani:** Writing – original draft, Supervision, Data curation, Conceptualization.

Declaration of Competing Interest

The authors declare that they have no known competing financial interests or personal relationships that could have appeared to influence the work reported in this paper.

Data availability

Data will be made available on request.

Acknowledgements

This work was supported by MUR National Innovation Ecosystem-Recovery and Resilience Plan (PNRR) Italy-Vitality, Mission 4 Component 2 - M4C2 Investiment 1.5 - Call for tender No. 3277 of DATE 30 dicembre 2021 Italian Ministry of University, Award Number: ECS00000041, Project Title: “Innovation, digitalisation and sustainability for the diffused economy in Central Italy”, Concession Degree No. 1057 of DATE 23.06.2022 adopted by the Italian Ministry of University (CUP D73C22000840006) and by University “G. d’Annunzio” (CUP D55F21002470005).

Appendix A. Supporting information

Supplementary data associated with this article can be found in the online version at doi:10.1016/j.colsurfb.2024.114043.

References

[1] P. Liu, G. Chen, J. Zhang, A review of liposomes as a drug delivery system: current status of approved products, regulatory environments, and future perspectives, Molecules 27 (2022) 1372, https://doi.org/10.3390/molecules27041372.
[2] S. Andrade, M.J. Ramalho, J.A. Loureiro, M.C. Pereira, Liposomes as biomembrane models: biophysical techniques for drug-membrane interaction studies, J. Mol. Liq. 334 (2021) 116141, https://doi.org/10.1016/j.molliq.2021.116141.
[3] M. Edidin, Lipids on the frontier: a century of cell-membrane bilayers, Nat. Rev. Mol. Cell. Biol. 4 (2003) 414–418, https://doi.org/10.1038/nrm1102.
[4] D. Kashchiev, D. Exerova, Bilayer lipid membrane permeation and rupture due to hole formation, Biochim. Biophys. Acta 732 (1983) 133–145, https://doi.org/10.1016/0005-2736(83)90196-7.
[5] N.A.A. Suhaimi, S. Ahmad, S.M.N. Husna, M.E. Sarmiento, A. Acosta, M. N. Norazmi, J. Ibrahim, R. Mohamud, R. Kadir, Application of liposomes in the treatment of infectious diseases, Life Sci. 305 (2022) 120734, https://doi.org/10.1016/j.lfs.2022.120734.
[6] A. Jash, A. Ubeyitogullari, S.S.H. Rizvi, Liposomes for oral delivery of protein and peptide-based therapeutics: challenges, formulation strategies, and advances, J. Mater. Chem. B 9 (2021) 4773–4792, https://doi.org/10.1039/D1TB00126D.
[7] Y. Wang, L. Miao, A. Satterlee, L. Huang, Delivery of oligonucleotides with lipid nanoparticles, Adv. Drug Deliv. Rev. 87 (2015) 68–80, https://doi.org/10.1016/j.addr.2015.02.007.
[8] S. Parveen, S. Kumar, S. Pal, N.P. Yadav, J. Rajawat, M. Banerjee, Enhanced therapeutic efficacy of Piperlongumine for cancer treatment using nano-liposomes mediated delivery, Int. J. Pharm. 643 (2023) 123212, https://doi.org/10.1016/j.ijpharm.2023.123212.
[9] D. Guimarães, A. Cavaco-Paulo, E. Nogueira, Design of liposomes as drug delivery system for therapeutic applications, Int. J. Pharm. 601 (2021) 120571, https://doi.org/10.1016/j.ijpharm.2021.120571.
[10] W.H. Abuwatfa, N.S. Awad, W.G. Pitt, G.A. Husseini, Thermosensitive polymers and thermo-responsive liposomal drug delivery systems, Polymers 14 (2022) 925, https://doi.org/10.3390/polym14050925.
[11] D.-Y. Wang, G. Yang, H.C. van der Mei, Y. Ren, H.J. Busscher, L. Shi, Liposomes with Water as a pH-Responsive Functionality for Targeting of Acidic Tumor and Infection Sites, Angew. Chem. Int. Ed. 60 (2021) 17714–17719, https://doi.org/10.1002/anie.202106329.
[12] E. Redolfi Riva, E. Sinibaldi, A.F. Grillone, S. Del Turco, A. Mondini, T. Li, S. Takeoka, V. Mattoli, Enhanced in vitro magnetic cell targeting of doxorubicin-loaded magnetic liposomes for localized cancer therapy, Nanomaterials 10 (2020) 2104, https://doi.org/10.3390/nano10112104.
[13] L. Wu, J. Wang, N. Gao, J. Ren, A. Zhao, X. Qu, Electrically pulsatile responsive drug delivery platform for treatment of Alzheimer’s disease, Nano Res 8 (2015) 2400–2414, https://doi.org/10.1007/s12274-015-0750-x.
[14] C. Wang, R. Zhang, J. He, L. Yu, X. Li, J. Zhang, S. Li, C. Zhang, J.C. Kagan, J. M. Karp, R. Kuai, Ultrasound-responsive low-dose doxorubicin liposomes trigger mitochondrial DNA release and activate cGAS-STING-mediated antitumour immunity, Nat. Commun. 14 (2023) 3877, https://doi.org/10.1038/s41467-023-39607-x.
[15] H.I. Kilian, A.J. Pradhan, D. Jahagirdar, J. Ortega, G.E. Atilla-Gokcumen, J. F. Lovell, Light-triggered release of large biomacromolecules from porphyrin-phospholipid liposomes, Langmuir 37 (2021) 10859–10865, https://doi.org/10.1021/acs.langmuir.1c01848.
[16] H.A.M. Abdelmohsen, N.A. Copeland, J.G. Hardy, Light-responsive biomaterials for ocular drug delivery, Drug Deliv. Transl. Res. 13 (2023) 2159–2182, https://doi.org/10.1007/s13346-022-01196-5.
[17] C. Bombelli, G. Caracciolo, P. Di Profio, M. Diociaiuti, P. Luciani, G. Mancini, C. Mazzuca, M. Marra, A. Molinari, D. Monti, L. Toccacieli, M. Venanzi, Inclusion of a photosensitizer in liposomes formed by DMPC/gemini surfactant: correlation between physico-chemical and biological features of the complexes, J. Med. Chem. 48 (2005) 4882–4891, https://doi.org/10.1021/jm050182d.
[18] L. Socrier, C. Steinem, Photo-lipids: light-sensitive nano-switches to control membrane properties, ChemPlusChem 88 (2023) e2023002, https://doi.org/10.1002/cplu.202300203.
[19] D. Liu, S. Wang, S. Xu, H. Liu, Photocontrollable intermittent release of doxorubicin hydrochloride from liposomes embedded by azobenzene-contained glycolipid, Langmuir 33 (2017) 1004–1012, https://doi.org/10.1021/acs.langmuir.6b03051.
[20] J. Morstein, A.C. Impastato, D. Trauner, Photoswitchable Lipids, ChemBioChem 22 (2021) 73–83, https://doi.org/10.1002/cbic.202000449.
[21] S. Ma, T. Ogata, S. Kim, K. Kanie, A. Muramatsu, S. Kurihara, Photo-responsive properties of phospholipid vesicles including azobenzene-containing amphiphilic phosphates, Trans. Mater. Res. Soc. Jpn. 40 (2015) 153–158, https://doi.org/10.14723/tmrsj.40.153.
[22] X.-R. Wang, M.-P. Li, W.-R. Xu, D. Kuck, Photo and pH dual-responsive supramolecular vesicles based on a water-soluble tribenzotriquinacene and an azobenzene-containing amphiphile in water, Asian J. Org. Chem. 10 (2021) 567–570, https://doi.org/10.1002/ajoc.202000683.
[23] J.S. Boruah, D. Chowdhury, Liposome-azobenzene nanocomposite as photo-responsive drug delivery vehicle, Appl. Nanosci. 12 (2022) 4005–4017, https://doi.org/10.1007/s13204-022-02666-5.
[24] S.J. Wezenberg, L.-J. Chen, J.E. Bos, B.L. Feringa, E.N.W. Howe, X. Wu, M. A. Siegler, P.A. Gale, Photomodulation of transmembrane transport and potential by stiff-stilbene based bis(thio)ureas, J. Am. Chem. Soc. 144 (2022) 331–338, https://doi.org/10.1021/jacs.1c10034.
[25] M. Ghani, A. Heiskanen, J. Kajtez, B. Rezaei, N.B. Larsen, P. Thomsen, A. Kristensen, A. Žukauskas, M. Alm, J. Emnéus, Appl. Mater. Interfaces 13 (2021) 3591–3604, https://doi.org/10.1021/acsami.0c19081.
[26] P.R. Sahoo, Light responsive materials: properties, design, and applications, Chapter 5, Stimuli-Responsive Mater. Biomed. Appl., ACS Symp. . Ser. Vol. 1436 (2023) 101–127, https://doi.org/10.1021/bk-2023-1436.ch005.
[27] R.H. Bisby, C. Mead, C.G. Morgan, Active uptake of drugs into photosensitive liposomes and rapid release on UV photolysis, Photochem. Photobiol. 72 (2000) 57–61, https://doi.org/10.1562/0031-8655(2000)072<0057:auodip>2.0.co;2.
[28] R.H. Bisby, C. Mead, C.G. Morgan, Wavelength-programmed solute release from photosensitive liposomes, Biochem. Biophys. Res. Commun. 276 (2000) 169–173, https://doi.org/10.1006/bbrc.2000.3456.
[29] S. Crespi, N.A. Simeth, B. König, Heteroaryl azo dyes as molecular photoswitches, Nat. Rev. Chem. 3 (2019) 133–146, https://doi.org/10.1038/s41570-019-0074-6.
[30] O. Sadovski, A.A. Beharry, F. Zhang, G.A. Woolley, Spectral tuning of azobenzene photoswitches for biological applications, Angew. Chem. Int. Ed. 48 (2009) 1484–1486, https://doi.org/10.1002/anie.200805013.
[31] T. Muraoka, K. Kinbara, Y. Kobayashi, T. Aida, Light-driven open−close motion of chiral molecular scissors, J. Am. Chem. Soc. 125 (2003) 5612–5613, https://doi.org/10.1021/ja034994f.

[32] Z.F. Liu, K. Hashimoto, A. Fujishima, Photoelectrochemical information storage using an azobenzene derivative, Nature 347 (1990) 658–660, https://doi.org/10.1038/347658a0.
[33] V. Balzani, A. Credi, M. Venturi, Molecular Devices and Machines: A Journey into the Nano World, Wiley-VCH: Weinheim, Germany, 2003, https://doi.org/10.1002/3527601600.
[34] J.E. Warias, F. Reise, S.C. Hövelmann, R.P. Giri, M. Röhrl, J. Kuhn, M. Jacobsen, K. Chatterjee, T. Arnold, C. Shen, S. Festersen, A. Sartori, P. Jordt, O. M. Magnussen, T.K. Lindhorst, B.M. Murphy, Photoinduced bidirectional switching in lipid membranes containing azobenzene glycolipids, Sci. Rep. 13 (2023) 11480, https://doi.org/10.1038/s41598-023-38336-x.
[35] P. Urban, S.D. Pritzl, M.F. Ober, C.F. Dirscherl, C. Pernpeintner, D.B. Konrad, J. A. Frank, D. Trauner, B. Nickel, T. Lohmueller, A Lipid Photoswitch Controls Fluidity in Supported Bilayer Membranes, Langmuir 36 (2020) 2629–2634, https://doi.org/10.1021/acs.langmuir.9b02942.
[36] C. Pernpeintner, J.A. Frank, P. Urban, C.R. Roeske, S.D. Pritzl, D. Trauner, T. Lohmüller, Light-controlled membrane mechanics and shape transitions of photoswitchable lipid vesicles, Langmuir 33 (2017) 4083–4089, https://doi.org/10.1021/acs.langmuir.7b01020.
[37] P. Urban, S.D. Pritzl, D.B. Konrad, J.A. Frank, C. Pernpeintner, C.R. Roeske, D. Trauner, T. Lohmüller, Light-controlled lipid interaction and membrane organization in photolipid bilayer vesicles, Langmuir 34 (2018) 13368–13374, https://doi.org/10.1021/acs.langmuir.8b03241.
[38] S.D. Pritzl, P. Urban, A. Prasselsperger, D.B. Konrad, J.A. Frank, D. Trauner, T. Lohmüller, Photolipid bilayer permeability is controlled by transient pore formation, Langmuir 36 (2020) 13509–13515, https://doi.org/10.1021/acs.langmuir.0c02229.
[39] N. Chander, J. Morstein, J.S. Bolten, A. Shemet, P.R. Cullis, D. Trauner, D. Witzigmann, Optimized photoactivatable lipid nanoparticles enable red light triggered drug release, Small 17 (2021) 2008198, https://doi.org/10.1002/smll.202008198.
[40] H. Xiong, K.A. Alberto, J. Youn, J. Taura, J. Morstein, X. Li, Y. Wang, D. Trauner, P. A. Slesinger, S.O. Nielsen, Z. Qin, Optical control of neuronal activities with photoswitchable nanovesicles, Nano Res 16 (2023) 1033–1041, https://doi.org/10.1007/s12274-022-4853-x.
[41] Y. Liu, X. An, Preparation, microstructure and function of liposome with light responsive switch, Colloids Surf. B 178 (2019) 238–244, https://doi.org/10.1016/j.colsurfb.2018.10.068.
[42] T. Leinders-Zufall, U. Storch, K. Bleymehl, M. Mederos y Schnitzler, J.A. Frank, D. B. Konrad, D. Trauner, T. Gudermann, F. Zufall, PhoDAGs enable optical control of diacylglycerol-sensitive transient receptor potential channels, Cell Chem. Biol. 25 (2018) 215–223.e3, https://doi.org/10.1016/j.chembiol.2017.11.008.
[43] J.H.A. Folgering, J.M. Kuiper, A.H. de Vries, J.B.F.N. Engberts, B. Poolman, Lipid-mediated light activation of a mechanosensitive channel of large conductance, Langmuir 20 (2004) 6985–6987, https://doi.org/10.1021/la048942v.
[44] J.A. Frank, M. Moroni, R. Moshourab, M. Sumser, G.R. Lewin, D. Trauner, Photoswitchable fatty acids enable optical control of TRPV1, Nat. Commun. 6 (2015) 7118, https://doi.org/10.1038/ncomms8118.
[45] M. Lichtenegger, O. Tiapko, B. Svobodova, T. Stockner, T.N. Glasnov, W. Schreibmayer, D. Platzer, G.Guedes de la Cruz, S. Krenn, R. Schober, N. Shrestha, R. Schindl, C. Romanin, K. Groschner, An optically controlled probe identifies lipid-gating fenestrations within the TRPC3 channel, Nat. Chem. Biol. (4) (2018) 396–404, https://doi.org/10.1038/s41589-018-0015-6.
[46] A. Kowalczyk, M. Przychodna, S. Sopata, A. Bodalska, I. Fecka, Thymol and thyme essential oil—new insights into selected therapeutic applications, Molecules 25 (2020) 4125, https://doi.org/10.3390/molecules25184125.
[47] K. Kachur, Z. Suntres, The antibacterial properties of phenolic isomers, carvacrol and thymol, Crit. Rev. Food Sci. Nutr. 60 (2020) 3042–3053, https://doi.org/10.1080/10408398.2019.1675585.
[48] X. Wang, L. Tian, J. Fu, S. Liao, S. Yang, X. Jia, G. Gong, Evaluation of the membrane damage mechanism of thymol against Bacillus cereus and its application in the preservation of skim milk, Food Control 131 (2022) 108435, https://doi.org/10.1016/j.foodcont.2021.108435.
[49] L.A. Sampaio, L. Tairiny Santos Pina, M. Russo Serafini, D. dos Santos Tavares, A. Gibara Guimarães, Antitumor effects of carvacrol and thymol: a systematic review, Front. Pharmacol. 12 (2021) 702487, https://doi.org/10.3389/fphar.2021.702487.
[50] S.S. Swain, S.K. Paidesetty, R.N. Padhy, Synthesis of novel thymol derivatives against MRSA and ESBL producing pathogenic bacteria, Nat. Prod. Res. 33 (2019) 3181–3189, https://doi.org/10.1080/14786419.2018.1474465.
[51] R. Zappacosta, M. Aschi, A. Ammazzalorso, P. Di Profio, A. Fontana, G. Siani, Embedding calix[4]resorcinarenes in liposomes: Experimental and computational investigation of the effect of resorcinarene inclusion on liposome properties and stability, Biochim. Biophys. Acta Biomembr. 1861 (2019) 1252–1259, https://doi.org/10.1016/j.bbamem.2019.04.010.
[52] R. Zappacosta, M. Semeraro, M. Baroncini, S. Silvi, M. Aschi, A. Credi, A. Fontana, Liposome destabilization by a 2, 7-diazapyrenium derivative through formation of transient pores in the lipid bilayer, Small 6 (2010) 952–959, https://doi.org/10.1002/smll.200902306.
[53] S. Pilato, M. Aschi, M. Bazzoni, F. Cester Bonati, G. Cera, S. Moffa, V. Canale, M. Ciulla, A. Secchi, A. Arduini, A. Fontana, G. Siani, Biochim, Biophys. Acta Biomembr. 1863 (2021) 183667, https://doi.org/10.1016/j.bbamem.2021.183667.
[54] D. Van der Spoel, E. Lindahl, B. Hess, G. Groenhof, A.E. Mark, H.J.C. Berendsen, GROMACS: fast, flexible, and free, J. Comput. Chem. 26 (2005) 1701–1718, https://doi.org/10.1002/jcc.20291.
[55] W.F. Van Gunsteren, S.R. Billeter, A.A. Eising, P.H. Hunenberger, P. Kruger, A.E. Mark, W.R.P. Scott, I.G. Tironi, Biomolecular Simulation: The GROMOS96 Manual and User Guide Zurich Hochschulverlag AG an der ETH Zurich, Switzerland, 1996.
[56] A.K. Malde, L. Zuo, M. Breeze, M. Stroet, D. Poger, P.C. Nair, C. Oostenbrink, A. E. Mark, An Automated force field Topology Builder (ATB) and repository: version 1.0, J. Chem. Theory Comput. 7 (2011) 4026–4037, https://doi.org/10.1021/ct200196m.
[57] M.J. Frisch, G.W. Trucks, H.B. Schlegel, G.E. Scuseria, M.A. Robb, J.R. Cheeseman, G. Scalmani, V. Barone, G.A. Petersson, H. Nakatsuji, X. Li, M. Caricato, A. V. Marenich, J. Bloino, B.G. Janesko, R. Gomperts, B. Mennucci, H.P. Hratchian, J. V. Ortiz, A.F. Izmaylov, J.L. Sonnenberg, D. Williams-Young, F. Ding, F. Lipparini, F. Egidi, J. Goings, B. Peng, A. Petrone, T. Henderson, D. Ranasinghe, V. G. Zakrzewski, J. Gao, N. Rega, G. Zheng, W. Liang, M. Hada, M. Ehara, K. Toyota, R. Fukuda, J. Hasegawa, M. Ishida, T. Nakajima, Y. Honda, O. Kitao, H. Nakai, T. Vreven, K. Throssell, J.A. Montgomery Jr., J.E. Peralta, F. Ogliaro, M. J. Bearpark, J.J. Heyd, E.N. Brothers, K.N. Kudin, V.N. Staroverov, T.A. Keith, R. Kobayashi, J. Normand, K. Raghavachari, A.P. Rendell, J.C. Burant, S.S. Iyengar, J. Tomasi, M. Cossi, J.M. Millam, M. Klene, C. Adamo, R. Cammi, J.W. Ochterski, R.L. Martin, K. Morokuma, O. Farkas, J.B. Foresman, D.J. Fox, Gaussian 16, Revision C.01, Gaussian, Inc, Wallingford CT, 2016.
[58] J.C. Berendsen, J.P.M. Postma, W.F. van Gunsteren, J. HermansInteraction Models for Water in Relation to Protein Hydration Dordrecht , Springer , Vol 14 , Intermolecular Forces. The Jerusalem Symposia on Quantum Chemistry and Biochemistry (Ed.), B. Pullman , in: 1981, in: 331–342.
[59] G. Bussi, D. Donadio, M. Parrinello, Canonical sampling through velocity rescaling, J. Chem. Phys. 126 (2007) 014101, https://doi.org/10.1063/1.2408420.
[60] B. Hess, P-LINCS: a parallel linear constraint solver for molecular simulation, J. Chem. Theory Comput. 4 (2007) 116–122, https://doi.org/10.1021/ct700200b.
[61] T. Darden, D. York, L. Pedersen, Particle mesh Ewald: an N•log(N) method for Ewald sums in large systems, J. Chem. Phys. 98 (1993) 10089–10092, https://doi.org/10.1063/1.464397.
[62] L. Vetráková, V. Ladányi, J. Al Anshori, P. Dvoák, J. Wirz, D. Heger, The absorption spectrum of cis-azobenzene, Photochem. Photobiol. Sci. 16 (2017) 1749–1756, https://doi.org/10.1039/C7PP00314E.
[63] B. Hiroaki, Hydrogen bonding effect on the electronic absorption spectrum of p-hydroxyazobenzene, Bull. Chem. Soc. Jpn 31 (1958) 169–172, https://doi.org/10.1246/bcsj.31.169.
[64] H.M.D. Bandara, S.C. Burdette, Photoisomerization in different classes of azobenzene, Chem. Soc. Rev. 41 (2012) 1809–1825, https://doi.org/10.1039/c1cs15179g.
[65] H.-B. Cheng, S. Zhang, J. Qi, X.-J. Liang, J. Yoon, Advances in application of azobenzene as a trigger in biomedicine: molecular design and spontaneous assembly, Adv. Mater. 33 (2021) 2007290, https://doi.org/10.1002/adma.202007290.
[66] H.M.D. Bandara, S. Cawley, J.A. Gascon, S.C. Burdette, Short-circuiting azobenzene photoisomerization with electron-donating substituents and reactivating the photochemistry with chemical modification, Eur. J. Org. Chem. (2011) 2916–2919, https://doi.org/10.1002/ejoc.201100216.
[67] N. Ma, Y. Wang, Z. Wang, X. Zhang, Polymer micelles as building blocks for the incorporation of azobenzene: enhancing the photochromic properties in layer-by-layer films, Langmuir 22 (2006) 3906–3909, https://doi.org/10.1021/la053441a.
[68] J. Liu, L. Yan, J. Wang, T. Li, H. Zhao, L. Li, S.F. Lincoln, R.K. Prud'homme, Xuhong Guo, Reversible photo-responsive vesicle based on the complexation between an azobenzene containing molecule and α-cyclodextrin, RSC Adv. 5 (2015) 32846, https://doi.org/10.1039/c5ra04597e.
[69] J.A. Kim, W. Long, J.C. Kim, Preparation of dimethylaminopropyl octadecanamide/stearic acid vesicles incorporating azobenzene and their UV-responsive release property, Colloid Polym. Sci. 299 (2021) 741–749, https://doi.org/10.1007/s00396-020-04806-1.
[70] V.N. Georgiev, A. Grafmüller, D. Bléger, S. Hecht, S. Kunstmann, S. Barbirz, R. Lipowsky, R. Dimova, Area increase and budding in giant vesicles triggered by light: behind the scene, Adv. Sci. 5 (2018) 1800432, https://doi.org/10.1002/advs.201800432.
[71] M. Aleksanyan, A. Grafmüller, F. Crea, V.N. Georgiev, N. Yandrapalli, S. Block, J. Heberle, R. Dimova, Photomanipulation of minimal synthetic cells: area increase, softening, and interleaflet coupling of membrane models doped with azobenzene-lipid photoswitches, Adv. Sci. 10 (2023) 2304336, https://doi.org/10.1002/advs.202304336.
[72] A.K. Sharma, A. Chatterjee, P. Purkayastha, Photophysical isomerization of liposomal bilayer-included caffeic acid phenethyl ester leading to membrane dehydration, Chem. Phys. Impact 6 (2023) 100232, https://doi.org/10.1016/j.chphi.2023.100232.
[73] C.-M. Lin, C.-S. Li, Y.-J. Sheng, D.T. Wu, H.-K. Tsao, Size-Dependent properties of small unilamellar vesicles formed by model lipids, Langmuir 28 (2012) 689–700, https://doi.org/10.1021/la203755v.
[74] S. Moffa, M. Aschi, M. Bazzoni, F. Cester Bonati, A. Secchi, P. Bruni, P. Di Profio, A. Fontana, S. Pilato, G. Siani, Synthesis, characterization, and computational study of aggregates from amphiphilic calix[6]arenes. Effect of encapsulation on degradation kinetics of curcumin, J. Mol. Liq. 368 (2022) 120731, https://doi.org/10.1016/j.molliq.2022.120731.
[75] K. Czamara, K. Majzner, M.Z. Pacia, K. Kochan, A. Kaczor, M. Baranska, Raman spectroscopy of lipids: a review, J. Raman Spectrosc. 46 (2015) 4–20, https://doi.org10.1002/jrs.4607.
[76] K. Gardikis, S. Hatziantoniou, K. Viras, M. Wagner, C. Demetzos, A DSC and Raman spectroscopy study on the effect of PAMAM dendrimer on DPPC model lipid

membranes, Int. J. Pharm. 318 (2006) 118–123, https://doi.org/10.1016/j.ijpharm.2006.03.023.
[77] A.A. Petruk, R.M.S. Álvarez, Structural changes induced by interactions between thyroid hormones and phospholipid membranes: a Raman Spectroscopy study, J. Raman Spectrosc. 44 (2013) 346–354, https://doi.org/10.1002/jrs.4205.
[78] L. Adriaenssens, C. Estarellas, A. Vargas Jentzsch, M. Martinez Belmonte, S. Matile, P. Ballester, Quantification of nitrate-π interactions and selective transport of nitrate using calix[4]pyrroles with two aromatic walls, J. Am. Chem. Soc. 135 (2013) 8324–8330, https://doi.org/10.1021/ja4021793.
[79] W.-L. Huang, X.-D. Wang, S. Li, R. Zhang, Y.-F. Ao, J. Tang, Q.-Q. Wang, D.-X. Wang, Anion transporters based on noncovalent balance including anion-π, hydrogen, and halogen bonding, J. Org. Chem. 84 (2019) 8859–8869, https://doi.org/10.1021/acs.joc.9b00561.
[80] W.-L. Huang, X.-D. Wang, Y.-F. Ao, Q.-Qi Wang, D.-X. Wang, Artificial chloride-selective channel: shape and function mimic of the ClC channel selective pore, J. Am. Chem. Soc. 142 (2020) 13273–13277, https://doi.org/10.1021/jacs.0c02881.
[81] J. Mareda, S. Matile, Anion–π slides for transmembrane transport, Chem. Eur. J. 15 (2009) 28–37, https://doi.org/10.1002/chem.200801643.